

FEM MODELING FOR PERFORMANCE EVALUATION OF AN ELECTROMAGNETIC ONCOLOGY DEEP HYPERTHERMIA APPLICATOR WHEN USING MONOPOLE, INVERTED T , AND PLATE ANTENNAS

C. J. Trujillo-Romero*, L. Leija, and A. Vera

Department of Electrical Engineering, Section of Bioelectronics, Cinvestav-IPN, Ave. Instituto Politecnico Nacional 2508, San Pedro Zacatenco, México D.F. 07360, México

Abstract—This study focuses on the evaluation of the performance of a rectangular waveguide for deep hyperthermia when different antennas are used. Although there are several models of hyperthermia applicators, there are no studies of the advantages of employing different antennas for waveguides used in deep seated tumor treatments. Monopole antennas are the most used radiating elements inside waveguides. Here, the modeling of a monopole and two new proposed antennas, inverted T and plate, in order to find their optimal performance is presented. Parameters like output power, SWR and transmission coefficient generated for each modeled antenna were calculated by using the finite element method. The antennas with the best performance were selected in order to model an applicator-phantom system, which was used to calculate the temperature distributions generated inside the muscle phantom. The models were based on Maxwell and bioheat equations. Finally, thermal distributions were obtained and compared. The results indicate that the plate antenna generated a better focusing. The SWR obtained was 1.25, the output power was 54.71 W of 66 W applied, and the 42°C isotherm had a size of 2 cm \times 2 cm.

1. INTRODUCTION

Oncology hyperthermia is one of the alternatives to treat tumors. The aim of oncology hyperthermia is to increase tissue temperature in order to destroy cancerous tumors without damaging healthy tissue. Current

Received 18 July 2011, Accepted 23 August 2011, Scheduled 1 September 2011

* Corresponding author: Citlalli Jessica Trujillo-Romero (ctrujillo@cinvestav.mx).

research shows that cancer cells are more sensitive to temperatures above 42°C than healthy cells [1–3]. One of the most often used heating sources is electromagnetic (EM) radiation (EM hyperthermia). Several types of applicators can be used in EM hyperthermia, e.g., horn antennas and waveguides. The operation of this kind of applicators is based on power absorption which produces temperature increase in tumors; however, there are different problems that need to be solved in order to focus and control EM energy deposition in tissues [4].

One of the main challenges in deep hyperthermia therapy is the design of new applicators. Although waveguides has been used for many years in EM hyperthermia, their improvement is still required. The improvement could be achieved by reducing the aperture dimensions, for example. Waveguide dimensions depend, among other factors, on frequency and dielectric filling. In general, the higher the frequency the lower the penetration depth; hence, by choosing a frequency which allows enough penetration depth and by filling the waveguide with an appropriate dielectric filling ($1 \leq \epsilon_r \leq 150$) [5], it is possible to design a small applicator without affecting the penetration depth. The improvement of applicators could be achieved also by using different antennas as radiator element.

In spite of the widespread use of some waveguide applicators for cancer treatments, up to date, the effect of employing different antennas in a waveguide has not been studied. Some waveguides used as hyperthermia applicators are the ridged waveguides, [6] the AMC-4 array [7] and the two tilted waveguide [8]; however, all of them are fed by monopole antennas [1, 6–8]. There are performance studies of monopoles proposed for ISM-band applications, which have been used in the design of feeders for microwave antennas [9, 10]. Studies of antennas that have similar geometry than that of the plate antenna [11] and the analysis of the coaxial-to-waveguide adaptor incorporating a disc-ended probe [12] are reported. Nevertheless, these studies were not carried out for waveguides used as applicators for cancer treatments.

On the other hand, nowadays there are different methods of modeling whose goal is to generate models of different multidisciplinary phenomena [13]. By using these multiphysic models, a hyperthermia system can be modeled. The challenge consists on determining the absorption power related to the temperature increase generated on the biological tissue by the applicator [14]. The modeling of hyperthermia applicators and treatments are still required due to their complexity and multidisciplinary nature.

In this paper, an analysis, based on the finite element method (FEM), of the improvement of a rectangular waveguide behavior is presented. This study is focused in two aspects: the reduction of

the aperture dimensions and the effect of using different antennas in the waveguide; this latter has never been studied in hyperthermia applicators. A study of three dielectric materials in order to compare their effects in aperture reduction is presented; an analysis of three antennas was carried out in order to know the effect of using an applicator fed by different antennas.

2. METHODS

2.1. Rectangular Waveguide Design Theory and Aperture Reduction

In order to calculate the rectangular waveguide aperture, the following equations are employed [15]:

$$a = \frac{1}{2f_c\sqrt{\mu_0\mu_r\varepsilon_0\varepsilon_r}} \quad (1)$$

$$b = \frac{a}{2} \quad (2)$$

where a and b are height and width of the waveguide aperture respectively [16], f_c is the cut-off frequency, ε_0 , ε_r , μ_0 and μ_r are the permeability and permittivity of free space and the material inside the waveguide, respectively.

The waveguide length is given by the wavelength equation:

$$\lambda = z = \frac{1}{f_c\sqrt{\mu_0\mu_r\varepsilon_r\varepsilon_0}} \quad (3)$$

It can be seen from Eqs. (1) and (3) that waveguide dimensions are associated not only to the permeability and permittivity of the dielectric material inside the waveguide, but also with the cut-off frequency. Hence, the use of different dielectric media to reduce the size of the waveguide was studied. The dielectric media were air, deionized water and titanium dioxide. Deionized water and titanium dioxide were chosen because of their high dielectric constants, while air was chosen in order to know the reduction ratio when media with high ε_r are used to calculate the applicator dimensions. Dimensions were computed in the frequency range from 85 MHz to 200 MHz. Although there are some studies concerning applicators which works at 70 and 343 MHz (for deep and superficial hyperthermia, respectively), here we propose another frequency range [8, 17]. These frequencies were proposed because it was necessary to find a compromise between aperture dimensions and penetration depth, which is limited by frequency. The main goal is to obtain a non-invasive focused applicator able to locally treat tumors at depths greater than 2 cm [18, 19].

2.2. FEM Antenna Modeling

This study proposes three different antennas (monopole, inverted T and plate antenna) that fed the waveguide by means of a coaxial cable. By using different antennas, it was possible to generate different temperature distributions. These temperature distributions will allow treating cancer tumors without damaging healthy tissue by focusing heating on a definite zone; normal tissue can be damaged because even though heating is directed to the tumor, it also affects surrounding healthy tissue (hot spots). Nowadays, the characteristics needed to ensure an efficient performance of hyperthermia applicators are adequate tumor heating, the concentration of energy on tumor, the non-generation of hot spots and the minimum power losses. These characteristics are related not only with the aperture dimensions but also with the antenna type and its dimensions, which are studied in this section.

The electrical length of a dipole or monopole antenna will resonate at a given frequency when its physical length is slightly lower than the length of half-wave theory. The RF energy travels through the antenna at a velocity lower than that of the radiated energy in free space because the antenna has a dielectric constant greater than that of free space. Because of the differences in velocity between the wave in free space and in the antenna, the physical length of the antenna no longer corresponds to its electrical length. This variation is caused by the creation of high potentials at the tips of the antenna.

Usually, this shortening is in the order of 5% lower than the electrical length of the antenna but there is a direct relationship between the diameter and the length of the element. A thin wire antenna has lower effects on wave velocity than an antenna with a large cross section. The effect of antenna circumference on wave velocity is illustrated in Fig. 1 [20]; however, this effect has been studied only for monopole and dipole antennas. Therefore, it was important to carry out a study on the relationship between diameter and length in each of proposed antennas in order to evaluate their performance.

Furthermore, finding a relationship between the radius and the length of each antenna was important because with these data the matching between the applicator and the RF system was improved. If the applicator and the RF system are perfectly matched, the highest power transmission will occur. Each antenna type was analyzed by varying diameter and length in order to obtain the dimensions which generated the best applicator performance. The implemented antenna dimension shifts were proposed because of three reasons: aperture dimensions restrict the antenna length, the N connector has a small area to place the antenna and, finally, the relationship between the

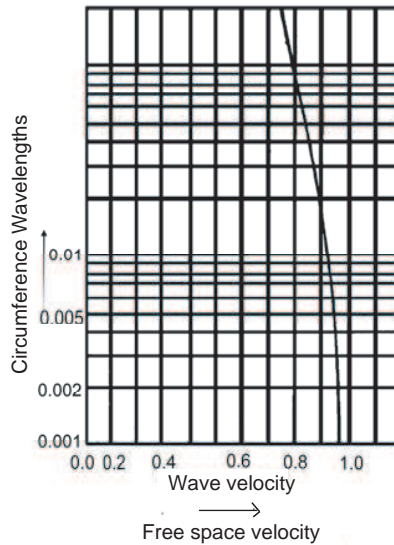


Figure 1. Effect of the antenna circumference on wave velocity [20].

antenna diameters and the maximum power must limit the heating of the antenna. Taking into account these considerations, a FEM model of the applicator with variations in radius and length of the antenna was designed.

2.2.1. Monopole Antenna

Figure 2 depicts the 3D model of the waveguide fed by the monopole antenna. The dielectric inside the waveguide was titanium dioxide because of its dielectric constant ($\epsilon_r = 90$). This relative permittivity allowed to reduce the applicator aperture and, as a consequence, the EM energy was concentrated in a small region.

In theory, the antenna length is a submultiple of lambda. However, there is a difference between the physical length of the antenna with its electrical length [15]. The discrepancy between these dimensions causes a mismatch and power losses in a hyperthermia system. If the hyperthermia system has power losses, more power will be needed in order to produce enough heating in tumor and more time may be necessary to achieve temperatures above 42°C. In order to find the real antenna dimensions and avoid power losses, the next shifts of antenna dimensions were implemented:

Shifts in the diameter of the monopole antenna: The length of the monopole antenna was $\lambda/6 = 2.68$ cm. The initial diameter antenna was 0.2 cm and it was varied up to 0.7 cm with increments of 0.1 cm.

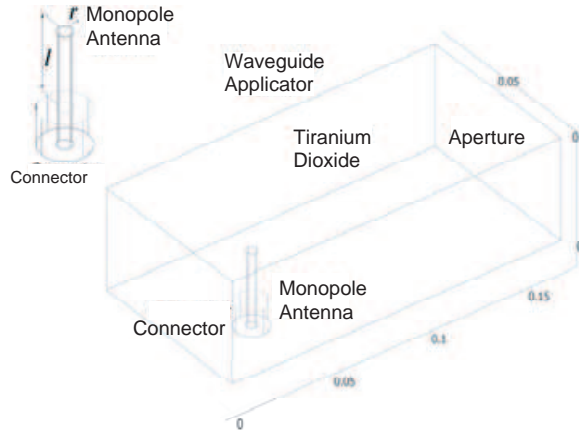


Figure 2. Waveguide fed by the monopole antenna; in this case, the shifts modeled were in antenna diameter and length. In the final model, the dielectric inside the applicator was titanium dioxide.

Shifts in the length of the monopole antenna: The considered diameter was 0.2 cm; the initial length was 1.9 cm and it was varied up to 3.1 cm with increments of 0.2 cm.

2.2.2. Inverted T Antenna

The second analysis was carried out for the applicator fed by the inverted T antenna. Fig. 3 depicts the 3D model with an inverted T antenna. In this analysis, it was also taken into account the antenna position: parallel and perpendicular to the direction of wave propagation (see Fig. 3). The radius used in all the models was 0.1 cm. In these models, only shifts of l and l_1 were implemented. Shifts of l varied from 2.1 cm to 3.7 cm with increments of 0.2 cm. Finally, the implemented shifts of l_1 varied from 2.1 cm to 4.5 cm with increments of 0.2 cm.

2.2.3. Plate Antenna

The plate antenna is shown in Fig. 4 where the 3D model is represented. The radius used in all the models was 0.1 cm. Here, shifts of l , l_1 and r_1 were implemented. Shifts of l varied from 1.6 cm to 3.0 cm with increments of 0.2 cm. Shifts of l_1 were from 0.2 cm to 0.8 cm with increments of 0.2 cm. Finally, r_1 was modified from 0.15 cm to 0.85 cm with increments of 0.2 cm.

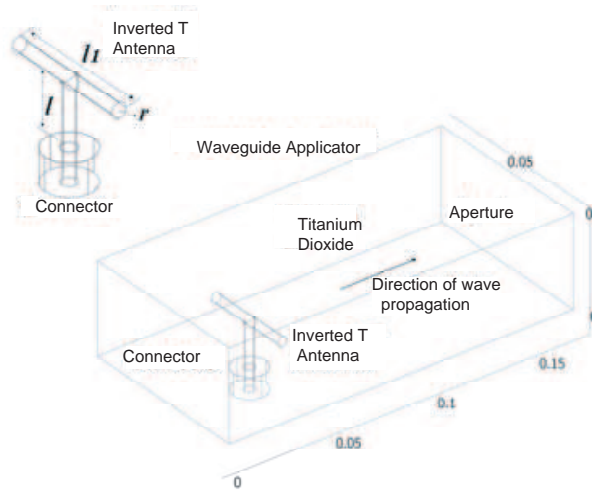


Figure 3. Waveguide fed by the inverted T antenna. This model considered the antenna oriented in perpendicular and parallel direction to the wave propagation. The shifts implemented were in l , l_1 while $r = 0.1$ cm. In the final model, the dielectric inside the applicator was titanium dioxide.

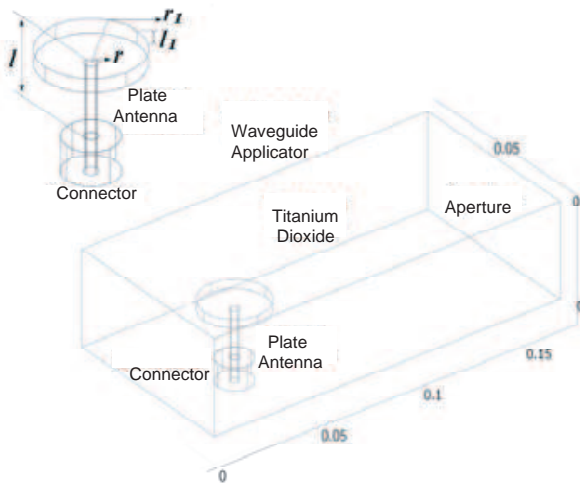


Figure 4. Waveguide fed by the plate antenna. The shifts considered in this model were in l , l_1 and r_1 while $r = 0.1$ cm. In the final model, the dielectric inside the applicator

2.3. FEM Modeling: Characteristics of the System and Validation by the Calculation of Power Losses

The waveguide walls were considered as perfect electric conductors (PEC boundary condition). The rectangular waveguide port was excited by a transverse electric (TE) wave. The TE mode was chosen because the electric field generated by the applicator could produce a temperature increase in tissue. If the applicator is polarized according to a TE₁₀ mode, the electric field is known analytically to be [15, 16]:

$$E = (0, 0, \sin(\pi(a - y)/(2a))) \cos(\omega t) \quad (4)$$

In order to work with 3D electromagnetic wave models, time-harmonic wave propagation can be used. This means that then the incident field has the form:

$$E = (0, 0, E_{0z}) = (0, 0, \sin(\pi(a - y)/(2a))) \quad (5)$$

Equation (5) describes the incident field generated by the applicator. The applicator can be considered as a network of two ports in order to analyze the behavior of electric field waves. Each port was defined with different characteristics, but both of them were considered for each modeled applicator. The first one was the entry port and it corresponds to the coaxial input of the applicator. This port was excited with 66 W. Waveguide applicators described by a similar work-teams reported power levels from 100 W to 300 W [21, 22]. However, in our study it was possible to use lower power levels, probably because our system was better coupled. The second port was the output port, which was considered as a rectangular waveguide.

Two-port networks are characterized by a number of equivalent circuit parameters such as their scattering matrix. The scattering matrix relates the outgoing waves b_1 and b_2 to the incoming waves a_1 and a_2 that converge on the two-ports. The scattering matrix is determined by Eq. (6) [23, 24].

$$\begin{bmatrix} b_1 \\ b_2 \end{bmatrix} = \begin{bmatrix} S_{11} & S_{12} \\ S_{21} & S_{22} \end{bmatrix} \begin{bmatrix} a_1 \\ a_2 \end{bmatrix}, \quad S = \begin{bmatrix} S_{11} & S_{12} \\ S_{21} & S_{22} \end{bmatrix} \quad (6)$$

where S_{11} , S_{22} refers to reflection coefficients, and S_{21} , S_{12} , to transmission coefficients. Finally, the standing wave ratio (SWR) is also related to the reflection coefficient Γ , which is obtained by the scattering matrix. The SWR is defined as the ratio of the maximum amplitude of the standing wave to the minimum amplitude. The SWR can be written as [17]:

$$\text{SWR} = \frac{1 + \Gamma}{1 - \Gamma} \quad (7)$$

where Γ (which can take the value of S_{11} or S_{22}) is the magnitude of the reflection coefficient. By using transmission coefficient and SWR it is possible to characterize each applicator.

Under ideal conditions, in which power losses caused by electrical resistance and imperfections in the dielectric material are neglected, all the RF power is transmitted from the generator to the load. In general, the higher the ratio of reflected power to forward power, the greater the SWR. When the SWR is high, the power loss is greater than the loss that occurs when the SWR is 1 (The SWR is always greater or equal to one). The transmission coefficient was also obtained. This coefficient is used when the wave propagation in a medium containing discontinuities is considered. These parameters were obtained, by modeling, for the applicator fed by each antenna type with different dimensions in order to predict power losses due to the mismatch in the hyperthermia system. The grid used for these models consisted of 11510 tetrahedral elements (which correspond to 15029 degrees of freedom); for this study we chose COMSOL Multiphysics V3.5, which is based on the finite element method, as a simulation software.

2.4. FEM Modeling of a Whole Hyperthermia System (Applicator-Phantom)

In order to model the hyperthermia treatment system, a muscle phantom irradiated by the applicator fed by each antenna obtained in the previous analysis was considered. For this purpose, it was necessary to use the bioheat equation which models heat transfer within tissue. The bioheat equation involves a spatial heating source. This source is useful when an external energy supply, such as an electromagnetic field, is used. The 3D model of the hyperthermia system is depicted in Fig. 5. The mesh grid comprised 9861 tetrahedral elements (21386 degrees of freedom) with a finer mesh in the antenna region.

The bioheat transfer equation proposed by Pennes [25, 26] can be written as:

$$\rho C \frac{\partial T}{\partial t} + \nabla \cdot (-k \nabla T) = \rho_b C_b \omega_b (T_b - T) + Q_{met} + Q_{ext} \quad (8)$$

where ρ is the tissue density, C is the specific heat of tissue, k is the tissue thermal conductivity, ρ_b is the blood density, C_b is the specific heat of blood, ω_b is the blood perfusion rate, T_b is the arterial blood temperature, Q_{met} is the heat source from metabolism and Q_{ext} is the spatial heat source, which is related to the EM field generated by the applicator. Q_{ext} is defined by the Eq. (9):

$$Q_{ext} = \frac{1}{2} \sigma_t |E|^2 \quad (9)$$

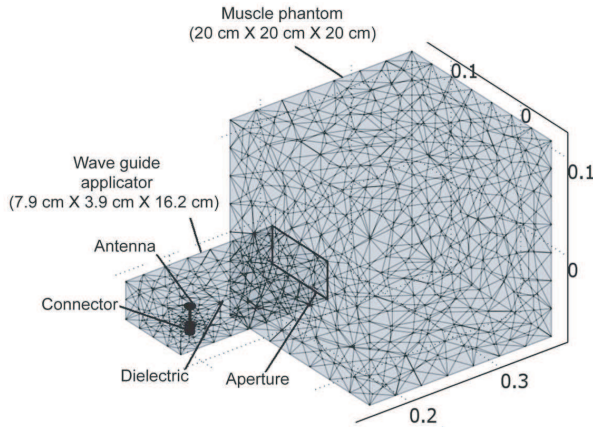


Figure 5. 3D Model of the applicator and muscle phantom. The model considered three different types of antennas: monopole, inverted T and plate. In the final model, the applicator is filled with titanium dioxide as dielectric material.

where σ_t is the electrical conductivity of the tissue, and E is the electric field generated by the WG applicator. The E field is described by Eq. (5), which was obtained by means of the application of the boundary conditions for Maxwell equations.

The properties of the muscle tissue used in the model are listed in Table 1. Relative permittivity and electrical conductivity depend on the frequency; therefore, these are specific values for 200 MHz. In our model, the metabolic heat source was considered as negligible. Finally, the special heat source was related to the electric field generated by our applicator, which is represented by Q_{av_rfw} .

By solving Eqs. (5) and (8) by FEM, it was possible to predict the interaction of electric field with tissue and to obtain temperature distributions inside the phantom. Temperature distributions at different Parallel and perpendicular planes respect to the position of the applicator were obtained and analyzed in order to predict the heating area. Parallel plane distributions were obtained in order to analyze the behavior of this applicator at greater depths (> 2 cm). In accordance with the definition of depth penetration [27] (See Eq. (10)), the penetration reached, in muscle tissue, should be approximately 6 cm. However, because the bioheat equation includes diverse parameters as blood perfusion rate, specific heat of blood, etc., the temperature reached in the muscle tissue at such depth might not

Table 1. Muscle properties used for the phantom model [28].

Property	Muscle
Thermal conductivity of tissue, k (W/mK)	0.5
Density of tissue, ρ (Kg/m ³)	1050
Specific heat of tissue, C (J/KgK)	3639
Density of blood, ρ_b (Kg/m ³)	1000
Specific heat of blood, C_b (J/KgK)	4180
Blood perfusion rate, ω_b (1/s)	0.0064
Arterial blood temperature, T_b (K)	310.15
Metabolic heat source, Q_{met} (W/m ³)	0
Spatial heat source, Q_{ext} (W/m ³)	Q_{av_rfw}
Relative permittivity, $\epsilon_r@200$ MHz	60.228
Electrical conductivity, σ (S/m)@200 MHz	0.74307

be in the therapeutic range.

$$\delta = \frac{1}{\omega} \left[\frac{\mu_0 \epsilon_r \epsilon_0}{2} \sqrt{1 + \left(\frac{\sigma}{\omega \epsilon} \right)^2} - 1 \right]^{-1/2} \quad (10)$$

3. RESULTS AND DISCUSSION

3.1. Waveguide Design Theory and Aperture Reduction

Table 2 and Fig. 6 show the applicator dimensions obtained for each dielectric media: air, deionized water and titanium dioxide. An applicator filled with air resulted totally inappropriate (see Table 2) for oncology therapies due to its excessive dimensions. Dimensions obtained with air did not allow energy to focus on the tumor. The applicator filled with deionized water was suitable for cancer treatments because at 200 MHz the energy could be focused more specifically on the tumor due to its small aperture dimensions: $a = 8.4$ cm, $b = 4.2$ cm and $z = 16.9$ cm. Even at the highest frequency (200 MHz) considered for this study, penetration depth was not affected because the wave penetration in muscle tissue was approximately 6.2 cm [28]. Finally, titanium dioxide presented the best results: the dimensions were $a = 7.9$ cm, $b = 3.9$ cm and $z = 16.1$ cm. These last results were achieved because of the high permittivity of titanium dioxide.

Analyzing Fig. 6 and Table 2, it can be observed how dielectric medium inside the applicator modifies its dimensions. For the

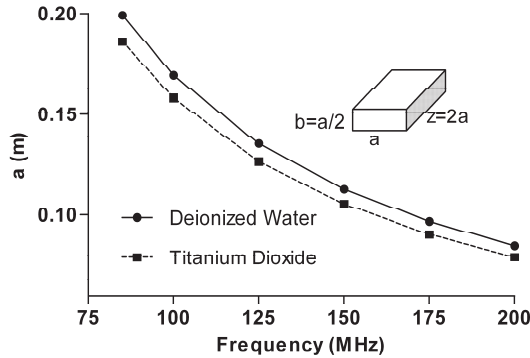


Figure 6. Waveguide dimensions calculated by using deionized water and titanium dioxide as dielectric materials.

Table 2. Waveguide dimensions calculated by using air as dielectric material inside.

Frequency (MHz)	Waveguide dimensions		
	a (m)	b (m)	z (m)
85	1.76	0.88	3.53
100	1.49	0.74	3.00
125	1.19	0.59	2.40
150	0.99	0.49	2.00
175	0.85	0.42	1.71
200	0.74	0.37	1.50

applicator filled with water, the reduction rate obtained was 8.5 while the reduction rate obtained with titanium dioxide was 10 with respect to water at 200 MHz. Achieving a 10-fold reduction of the aperture dimensions was suitable for hyperthermia applications because penetration deep was not affected and heat was focused. The best applicator dimensions were obtained with titanium dioxide; therefore it was used to model the applicator fed by the proposed antennas.

3.2. FEM Antenna Modeling

In this section, the results of the first study of how dimensions of a monopole antenna and two new proposed antennas (plate and inverted

T antennas) affect the linkage level from generator to waveguide are presented. The best linkage in our system ($\text{SWR} \sim 1$) improved the power transmission and avoided standing waves capable of damaging the RF equipment. This analysis was achieved by obtaining the SWR, output power and transmission coefficient generated by each antenna.

3.2.1. Monopole Antenna

a) Shifts in diameter of the monopole antenna

Figure 7 depicts the SWR at the input (coaxial cable and connector) and the SWR at the output of the rectangular waveguide. We observed that if the antenna diameter decreased, so did the SWR. This was because the antenna material (copper) helped increase or decrease the linkage levels of the generator with the waveguide; as a result, an increase or a decrease in transmitted power was observed.

Table 3 shows the input and the output SWR at critical diameters. Critical diameters were considered as the smallest, the biggest, and one that could be adapted by a matching network, e.g., a stub. From these results, it was observed that if the antenna diameter increased, there was a bigger mismatch for the input and for the output as well. It is necessary to remember that SWR values should be maintained between 1 and 1.2; this parameter (SWR) indicates an appropriate level of the system matching. If an antenna diameter bigger than 0.3 cm (input $\text{SWR} \leq 1.66$ and output $\text{SWR} \geq 2.25$) was used, the level of mismatch increased; these levels of mismatch provoked that part of the energy was not to be radiated and therefore the efficiency decreased. Reflected power causes heat to increase at the RF system which can be damaged depending on the magnitude of the SWR.

Figure 8 represents the transmission coefficient and the output power as function of different diameters in the monopole antenna. It was observed that there was a transmission coefficient of 0.84 with an antenna diameter of 0.2 cm and only 0.47 with an antenna diameter of 0.7 cm. Analyzing Figs. 7 and 8, it is clear that if the SWR is close to

Table 3. Input and output SWR at the critical diameters of the applicator fed by the monopole antenna when using titanium dioxide as dielectric inside the applicator.

Antenna Diameter (cm)	Input SWR (Coaxial cable)	Output SWR (waveguide aperture)
0.2	1.00	1.65
0.3	1.66	2.25
0.7	9.75	7.11

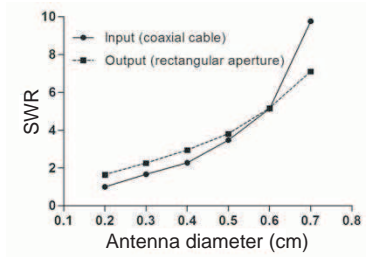


Figure 7. SWR of the applicator fed by the monopole antenna as a function of the antenna diameter. The input SWR was considered as the SWR at the coaxial cable-monopole antenna interface while the output SWR was considered as the SWR at the end of the applicator (rectangular aperture).

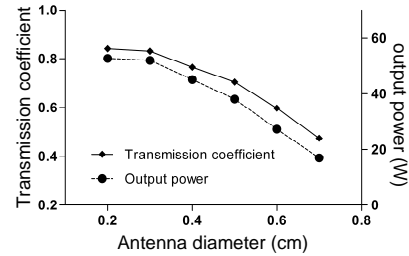


Figure 8. Transmission coefficient and output power of the applicator fed by the monopole antenna as a function of the antenna diameter.

1, between 70% and 80% of power is transmitted from port 1 (input) to port 2 (output). The maximum output power, 52.62 W of a total of 66 W, was obtained with the smallest diameter (0.2 cm). The output power decreased to 16.94 W when using a diameter of 0.7 cm. Finally, we observed that if the monopole length was 2.63 cm ($\lambda/6$), the best diameter antenna was 0.2 cm because the SWR, the output power, and the transmission coefficient were better than those obtained with other diameters.

b) Shifts in length of the monopole antenna

The second analysis was carried out by varying the monopole antenna length. Fig. 9 represents the input and output SWR of an antenna length between 1.9 cm–3.5 cm and a radius of 0.1 cm. The obtained SWR varied from 1.3 to 1.6 at the input and from 1.6 to 1.8 at the output. These relations indicate a close-to-ideal level of linkage in our system; however, when taking the intersection point of curves, SWR input and output, the antenna dimensions were $d = 0.2$ cm and $l = 2.35$ cm; then, the obtained SWR was 1.2 and therefore the linkage level was optimum. Although we can see two intersection points in the curves (see Fig. 9), the first point at $l = 2$ cm has a greater SWR (1.4); for this reason, the second point was chosen.

Figure 10 shows transmission coefficient and output power at different monopole antenna lengths. According to Fig. 10, the antenna length between 2.2 cm–2.7 cm had a performance that ensured a good power transmission because these dimensions allowed a transmission

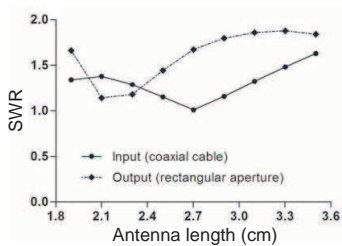


Figure 9. SWR of the applicator fed by the monopole antenna as a function of the antenna length. The input SWR was considered as the SWR at the coaxial cable-monopole antenna interface while the output SWR was considered as the SWR at the end of the applicator (rectangular aperture).

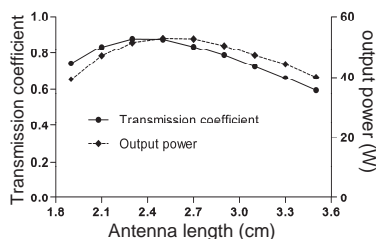


Figure 10. Transmission coefficient and output power of the applicator fed by the monopole antenna as a function of the antenna length l .

of 72%–80% of the input power; nevertheless, an antenna length of 2.35 cm showed the maximum power transmission: 80% of the input power.

In summary, for the monopole antenna case, it was observed that the level of mismatch was reduced and the power transmission increased (80% of the input power) by using a small diameter (0.2 cm) and a length between 2.35 cm and 2.5 cm.

3.2.2. Inverted T Antenna

a) Perpendicular inverted T antenna

Figure 11 represents the SWR analysis for the perpendicular T antenna. Fig. 11 shows that if l was longer than 2 cm, the difference between input SWR and output SWR increased; therefore, the level of mismatch also increased and there were more power losses in the system. Even though the SWR values showed in Fig. 11 vary from 1 to 2.11, the difference between input and output SWR increased for each l_1 showed in Fig. 11. These differences indicate that even if the input SWR is near to 1, there are losses when the EM wave travels through the applicator. The maximum differences between input SWR and output SWR were 0.28 for $l_1 = 1$ cm, 0.35 for $l_1 = 2$ cm, 0.77 for $l_1 = 3$ cm and 1.11 for $l_1 = 4$ cm.

Table 4 represents the antenna dimensions for which the input and output SWR had the same values, i.e., the intersection between curves

having the same l_1 , and therefore for these dimensions the transmission power is near to the optimal value (almost all the power is transmitted). From this table it can be observed that if l_1 increases, the input and output SWR moves farther from the ideal value (SWR 1) causing an increased mismatch in the system. An SWR of 1.09 was obtained with the dimensions $l = 1.82$ cm, $l_1 = 2$ cm and $r = 0.1$ cm. These dimensions were chosen as optimal, even for modeling the system with muscle phantom, because when the SWR was approximately 1, the power loss was smaller than the loss that occurred when the SWR was higher.

In Fig. 12, the transmission coefficients are plotted. The maximum transmission coefficients obtained with $l_1 = 1.0$ cm and $l_1 = 2.0$ cm were 0.85 and 0.83, respectively, when $l = 1.9$ and $l = 1.6$. These values allowed a good power transmission to our applicator because they occur

Table 4. Input and output SWR at the critical dimensions of the applicator fed by the perpendicular inverted T antenna when using titanium dioxide as dielectric inside the applicator.

Antenna Dimensions (cm)			Input SWR (Coaxial cable)	Output SWR (waveguide aperture)
l	l_1	r		
1.95	1	0.1	1.24	1.24
1.82	2	0.1	1.09	1.09
1.76	3	0.1	1.10	1.10
1.76	4	0.1	1.35	1.35

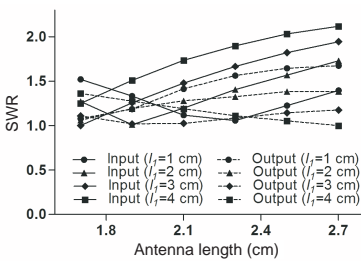


Figure 11. SWR of the applicator fed by the perpendicular inverted T antenna as a function of the antenna length l .

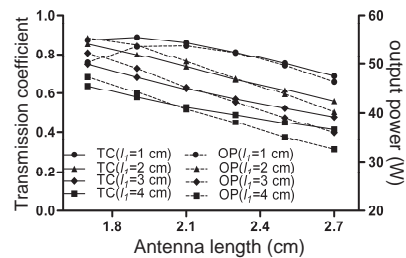


Figure 12. Transmission coefficient and output power of the applicator fed by the perpendicular inverted T antenna as a function of the antenna length l . TC = Transmission coefficient, OP = Output power.

when the SWR is near to the ideal value. In Fig. 12, the maximum output power, which was 55 W (when an input power = 66 W is applied), is also observed; it was obtained with $l_1 = 2.0$ cm and $l \sim 1.8$ cm. The output power was reduced if the antenna length l_1 increased.

b) Parallel inverted T antenna

Figure 13 shows the input and output SWR for the parallel T antenna. If l was greater than 2.0 cm, the differences between input SWR and output SWR were bigger; therefore, the mismatch of the system increased. Fig. 14 depicts the transmission coefficients and the output power of the parallel inverted T antenna. In this case, the antenna with the dimensions $l = 1.8$ cm and $l_1 = 2.0$ cm had an output power of 55.23 W and its transmission coefficient was 0.85. However, although the antenna with $l_1 = 2.0$ cm had an output power of 55.23 W, the antenna with $l_1 = 1.0$ cm and l higher than 1.9 cm also had a high output power between 52.0 and 53.7 W for a total input power of 66.0 W.

Table 5 represents the parallel inverted T antenna dimensions for which the input and output SWR had the same values, i.e., the intersection of the curves having the same SWR values (see Fig. 13). For these points there was almost a total transmission power. This table shows that if l_1 increased the input and output SWR decreased, thus which caused an increased mismatch in our system. It is observed that parallel antenna dimensions of $l = 1.81$ cm, $l_1 = 2.0$ cm and $r = 0.1$ cm had a SWR of 1.07 which, in practice, stands for an excellent matching.

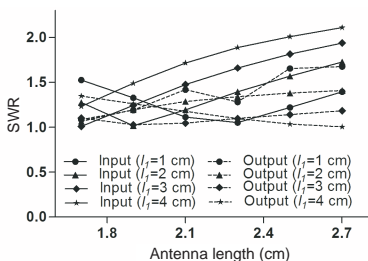


Figure 13. SWR of the applicator fed by the parallel inverted T antenna as a function of the antenna length l .

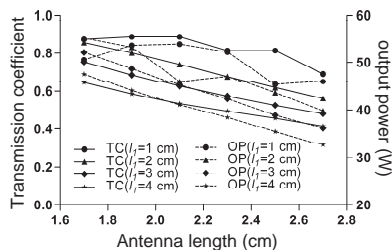


Figure 14. Transmission coefficient and output power of the applicator fed by the parallel inverted T antenna as a function of the antenna length l . TC = Transmission coefficient, OP = Output power.

3.2.3. Plate Antenna

Figure 15 shows the SWR for the plate antenna. If the diameter of r_1 is greater than 0.8 cm, the differences between input SWR and output SWR increased up to 50% between them, thus the mismatch of the system was greater. Analyzing Figs. 15 and 16, the antenna dimensions chosen for the next analysis, in which a muscle phantom was considered as a load, were $l = 1.9$ cm, $r = 0.1$ cm, $r_1 = 0.15$ cm and $l_1 = 0.15$ cm; an average SWR of 1.26 was obtained with these dimensions. The obtained transmission coefficient for these dimensions was 0.83 and the output power was 54.71 W; 82.8% of the input power was transmitted through the applicator when using these dimensions.

Table 5. Input and output SWR (at the intersection point) of the applicator fed by the parallel inverted T antenna when using titanium dioxide as dielectric inside the applicator.

Antenna Dimensions (cm)			Input SWR (Coaxial cable)	Output SWR (waveguide aperture)
l	l_1	r		
1.95	1	0.1	1.28	1.28
1.81	2	0.1	1.07	1.07
1.78	3	0.1	1.10	1.10
1.76	4	0.1	1.30	1.30

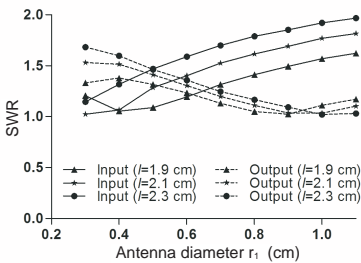


Figure 15. SWR of the applicator fed by the plate antenna as a function of the antenna length l with $r = 0.1$ cm.

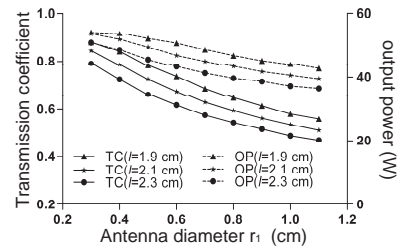


Figure 16. Transmission coefficient and output power of the applicator fed by the plate antenna as a function of the antenna length l with $r = 0.1$ cm. TC = Transmission coefficient, OP = Output power.

3.3. Modeling the Applicator when Radiating a Muscle Phantom

In this section, the results of the heating generated inside a muscle phantom when using the proposed antennas, (monopole, plate and inverted T) with their optimal dimensions described in the previous stage, are discussed. Nowadays, most of the commercialized external applicators are able to treat only superficial tumors (< 2 cm depth); therefore, this applicator was tested at 3.5 cm in order to assess if this applicator could be used to treat deeper tumors and to know the temperature behavior at greater depth. The antennas which had the best performance are presented in Table 6. Temperatures in a parallel plane to the antenna were obtained. For this analysis, there was a notable difference in the heating distribution generated by each applicator.

Figure 17 depicts the temperature distributions inside the muscle phantom ($20\text{ cm} \times 20\text{ cm}$) at 3.5 cm of depth. Figs. 17(a) and 17(b) show the temperature distributions generated by the monopole antenna. In both figures, distributions were similar and the difference

Table 6. Performance of the antennas which had an optimum SWR. A muscle phantom was included in the model at the aperture of the applicator. In these models titanium dioxide was selected as dielectric inside the applicator.

Antenna type	Dimensions (cm)	Input and output SWR	Transmission coefficient	Output power (W)
Monopole (shifts in diameter)	$l = 2.63,$ $r = 0.10$	1.00, 1.65	0.84	52.62
Monopole (shifts in length)	$l = 2.35,$ $r = 0.10$	1.20, 1.20	0.78	52.62
Perpendicular inverted T	$l = 1.82$ $l_1 = 2.00$ $r = 0.10$	1.09, 1.09	0.85	55.31
Parallel inverted T	$l = 1.81$ $l_1 = 2.00$ $r = 0.10$	1.07, 1.07	0.85	55.23
Plate antenna	$l = 1.90$ $l_1 = 0.15,$ $r = 0.10$ $r_1 = 0.15$	1.20, 1.33	0.83	54.71

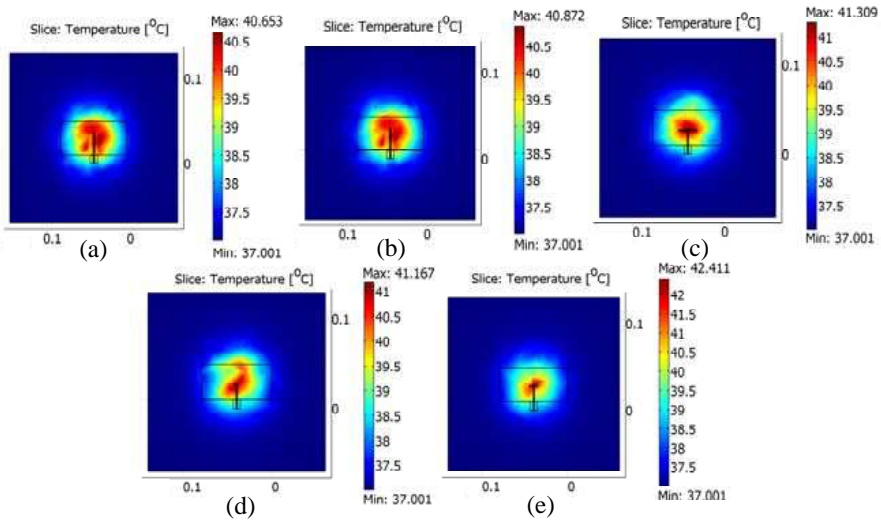


Figure 17. Parallel distributions of temperature at 3.5 cm of depth. (a) Monopole with variations in diameter. (b) Monopole with variations in length. (c) Perpendicular inverted T . (d) Parallel inverted T . (e) Plate antenna.

of maximum temperatures was 0.21°C . The 40.6°C isotherm had approximately a dimension of $6\text{ cm} \times 4\text{ cm}$. An important thing to consider is that this applicator could affect not only the tumor but also healthy tissue when used to treat small tumors ($\sim 2\text{ cm} \times \sim 2\text{ cm}$). However, it may be used to treat tumors in the range of 4 cm to 6 cm.

On the other hand, Figs. 17(c) and 17(d) depict the temperature distributions generated by the applicator fed by the inverted T antennas, perpendicular and parallel respectively. Although both distributions were generated by similar antennas, the perpendicular inverted T antenna presented a better distribution because of the circular-centered heating region. This region, isotherm 41°C , had a size of $4\text{ cm} \times 3\text{ cm}$ and it was focused at the center of the applicator. In Fig. 17(d) it can be observed that if the tumor is located in the central region, a parallel inverted T antenna might generate hot spots in other regions because the temperature is not focused at the center of the muscle phantom (the isotherm has an ellipsoidal shape). This unfocused distribution could be explained due to the direction of the antenna, which was parallel to the trajectory of the EM waves. In both cases, the maximum temperature was in the range between 41°C and 41.5°C . These temperatures were close to the 42°C needed to generate

hyperthermia but this temperature can be reached by varying time and power input.

Finally, Fig. 17(e) shows the temperature distributions generated by the plate antenna. This antenna presents better results because the region with the maximum temperature increases (isotherm 42°C) had approximately a size of $2\text{ cm} \times 2\text{ cm}$ and it was focused at the phantom center. This applicator may not generate hot spots in healthy tissue if used to treat a smaller tumor. A parallel plane at 3.5 cm of depth showed that the maximum temperature was 42.42°C .

Figure 18 shows the three cross-section planes generated by each proposed antenna. Figs. 18(a) and 18(b) depict the 3D cross-section generated by the monopole antenna with variations in diameter and length, respectively. Although both distributions are similar, reached temperature was greater (67.16°C) for the monopole antenna with variations in length; i.e., with this antenna, it is possible to improve the power transmission from the applicator to the muscle phantom. Figs. 18(c) and 18(d) show the results for perpendicular and parallel inverted T antennas, respectively. In this case, 3D distribution for

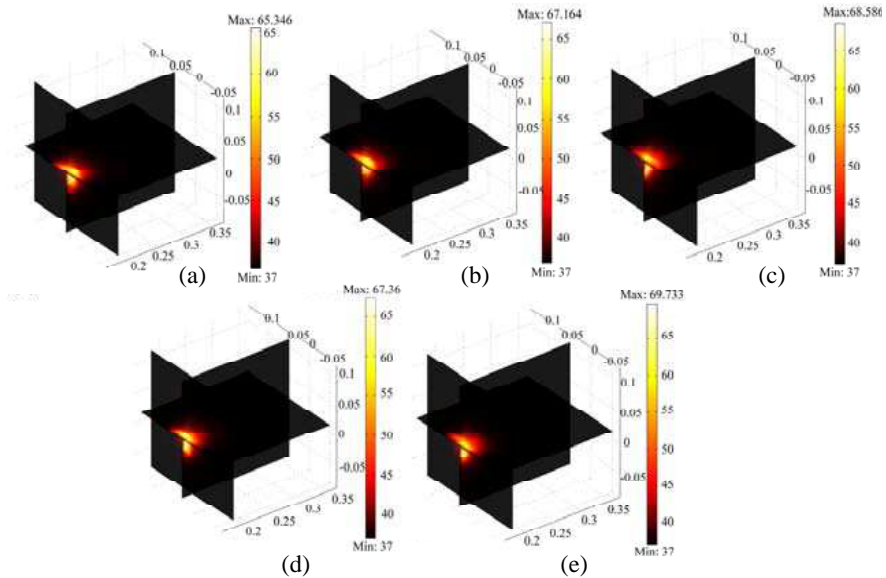


Figure 18. Three cross-section planes generated by each proposed antenna. (a) Monopole with variations in diameter. (b) Monopole with variations in length. (c) Perpendicular inverted T . (d) Parallel inverted T . (e) Plate antenna.

the perpendicular inverted T antenna showed a concentration of the highest temperature increments in a smaller region (this corroborated the results showed in Fig. 18(c)); moreover, this antenna reached temperatures up to 68.58°C (higher than those obtained with the monopole antenna). Finally, Fig. 18(e) depicts the 3D distribution obtained with the plate antenna; although this distribution looks very similar to that obtained for the perpendicular inverted T antenna (both distributions presented a high temperature concentration), with the plate antenna a maximum temperature of 69.73°C was reached (the highest in all the study).

Table 7 shows a comparison between the output power obtained by modeling the applicator with and without the muscle phantom. These data showed that when the muscle phantom was radiated, there were power losses, as expected. These power losses were due to the transition of the EM waves from the applicator to the muscle phantom.

In Table 7 it is possible to observe that even though the two monopole antennas had a very similar output power without phantom (52.62 W); the output power obtained in the last section was different. The monopole antenna with shifts in diameter had a difference of 4.04 W while the difference in the monopole antenna with shifts in length was 2.52 W . The other antennas had power losses of 5 W approximately. From this, we can conclude that the monopole antenna

Table 7. Comparison of the output power obtained with and without muscle phantom and percentage of the input power delivered when the phantom was included*. OP = Output power, IP = Input power.

Antenna type	OP obtained when the muscle phantom is not included in the model (W)	OP obtained when the muscle phantom is included in the model (W)	Efficiency, expressed in percentage, when the muscle phantom is included in the model
Monopole (shifts in ϕ)	52.62	48.61	73.0%
Monopole (shifts in l)	52.62	50.06	75.8%
Perpendicular inverted T	55.31	50.03	75.8%
Parallel inverted T	55.23	50.15	76.0%
Plate	54.71	49.39	74.8%

*Antenna dimensions can be seen on Table 6.

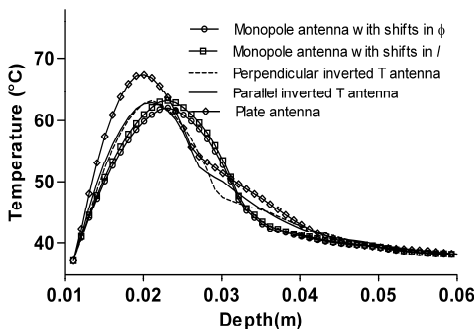


Figure 19. Temperature decrease as function of depth. Depth was limited to 5 cm even though the dimensions of the phantom were 20 cm.

with shifts in length had fewer losses; however, the EM energy was not focused. Even though the output power of the parallel inverted T antenna was 50.1 W (~ 5 W of loss), the isotherm 42°C was approximately $4\text{ cm} \times 3\text{ cm}$ and the distribution was not focused at the center of the muscle phantom (see Fig. 17(d)). Although the output power obtained with the plate antenna was 49.39 W (~ 5 W of loss), the affected region was the smallest ($2\text{ cm} \times 2\text{ cm}$); hence, the energy could be focused and the maximum temperature in this region was approximately 42°C at 3.5 cm of depth.

Figure 19 presents the temperature increase that occurred at the central plane of the muscle phantom perpendicular to the aperture of the applicator; temperature was assessed in relation to the phantom depth. Monopole and inverted T antennas generated similar temperatures; below 42°C at depths greater than 3.5 cm. On the other hand, the plate antenna was the only one that generated temperatures above 42°C at depths greater than 3.5 cm. Although the maximum temperatures obtained with each antenna were higher ($\sim 65^\circ\text{C}$), the temperature can be regulated, in practice, by using a water bolus between the applicator and the muscle phantom or by reducing the power level input ($< 66\text{ W}$).

4. CONCLUSIONS

This paper presents the modeling of an electromagnetic applicator (waveguide) for hyperthermia treatments which was modeled with three different antennas. The first one was a monopole antenna, which is broadly used in hyperthermia applicators; the others were two new proposed antennas: inverted T and plate antenna, for which there are

no reports of their use in hyperthermia. A study of different dielectric materials in order to use them inside the waveguide in order to reduce the aperture dimensions was also carried out. Materials analyzed were air, deionized water and titanium dioxide.

The study of aperture reduction consisted in using different dielectrics inside the applicator and in increasing the cut-off frequency. The analyses at different frequencies and with different materials inside the waveguide resulted in the election of the titanium dioxide which reduced the aperture dimensions by a factor of 10, compared to those obtained by using air inside the applicator. This aperture reduction allowed concentrating the energy over the tumor region. Although the applicator with dioxide titanium had the best aperture reduction, the applicator with deionized water achieved a reduction rate of 8.5. This factor of 8.5 allowed obtaining an applicator that can also be used in hyperthermia therapies for small cancer tumors.

The parameters obtained by the FEM antenna modeling (SWR, transmission coefficient and output power) showed that the dimensions of each antenna assure between 75%–80% of power transmission, taking into account that, in practice, a 100% transmission never occurs. This analysis was carried out in order to model a whole hyperthermia system with each antenna. Each applicator fed by the selected antennas was modeled in a whole hyperthermia system (phantom-applicator model). Temperature distributions generated by each applicator were compared in order to select the one which better focused the energy, allowed enough depth penetration and achieved enough temperature to induce hyperthermia.

The study of the whole hyperthermia system demonstrated that the use of a monopole antenna results in large heating areas (Isotherm 40°C), 6 cm × 4 cm, and losses of 26.4% of the input power. The most used antenna in all the analysis reported by other work-teams has been the monopole antenna; however, our results showed that antennas as the inverted T and plate antenna had better performance: they had a power transmission of 75.8% and 76% respectively. Even though the heating areas (isotherms 40°C) were similar (4 cm × 3 cm), heating generated by the parallel antenna was not focused compared with that generated by the perpendicular antenna (see Fig. 17(d)). Results demonstrated that although power transmission with plate antenna was only 75%, 1% below the inverted T antenna, the heating area was the smallest, ~ 2 cm × 2 cm (isotherm 42°C); this area offers the possibility to treat tumors between 1–2 cm of size. The results obtained show that a plate antenna is a better option for the design of EM applicators for oncology therapy when focalized and deep penetration heating is needed.

Finally, the optimal dimensions of each proposed antenna, under specific conditions, were obtained. The applicator fed by each antenna delivered the same power level (see Table 7) to the muscle phantom; however, different shapes of temperature distribution were obtained with each antenna; consequently, each applicator obtained can be used for different cancer therapies according to the size of the tumor. Currently, these models are being validated by means of measuring the temperature and the electric field distributions generated by the applicator (fed by each antenna) built with the dimensions obtained in this study.

ACKNOWLEDGMENT

This work was partially supported by the European Project ALFA — Contract N° AML/B7-311/97/0666/II-0343-FA-FCD-FI, and the Mexican projects Conacyt 45041 and 68799.

REFERENCES

1. Gardner, R. A., H. I. Vargas, J. B. Block, C. L. Vogel, A. J. Fenn, G. V. Kuehl, and M. Doval, “Focused microwave phased array thermotherapy for primary breast cancer,” *Annals of Surgical Oncology*, Vol. 9, 326–332, May 2002.
2. Lagendijk, J. J., “Hyperthermia treatment planning,” *Phys. Med. Biol.*, Vol. 45, R61–76, May 2000.
3. Sabariego, R. V., L. Landesa, and F. Obelleiro, “Design of a microwave array hyperthermia applicator with a semicircular reflector,” *Med. Biol. Eng. Comput.*, Vol. 37, 612–617, Sep. 1999.
4. Gupta, R. C. and S. P. Singh, “Elliptically bent slotted waveguide conformal focused array for hyperthermia treatment of tumors in curved region of human body,” *Progress In Electromagnetics Research*, Vol. 62, 107–125, 2006.
5. Cheung, A. Y. and A. Neyzari, “Deep local hyperthermia for cancer therapy: external electromagnetic and ultrasound techniques,” *Cancer. Res.*, Vol. 44, 4736s–4744s, Oct. 1984.
6. Kato, H. and T. Ishida, “Present and future-status of noninvasive selective deep heating using RF in hyperthermia,” *Med. Biol. Eng. Comput.*, Vol. 31, S2–S11, Jul. 1993.
7. Wiersma, J. and J. D. P. Van Dijk, “RF hyperthermia array modelling; validation by means of measured EM-field distributions,” *Int. J. Hyperthermia*, Vol. 17, 63–81, Jan. 2001.

8. Nilsson, P., T. Larsson, and B. Persson, "Absorbed power distributions from two tilted waveguide applicators," *Int. J. Hyperthermia*, Vol. 1, 29–43, Jan.–Mar. 1985.
9. Chen, Z. N., K. Hirasawa, and K. Wu, "A broad-band sleeve monopole integrated into parallel-plate waveguide," *IEEE Transactions on Microwave Theory and Techniques*, Vol. 48, 1160–1163, Jul. 2000.
10. Park, M. Y. and H. J. Eom, "Analysis of a coaxially fed monopole in a rectangular waveguide," *IEEE Microwave and Wireless Components Letters*, Vol. 15, 253–255, Apr. 2005.
11. Bialkowski, M. E., "On the link between top-hat monopole antennas, disk-resonator diode mounts and coaxial-to-waveguide transitions," *IEEE Transactions on Antennas and Propagation*, Vol. 48, 1011–1013, Jun. 2000.
12. Bialkowski, M. E., "Analysis of a coaxial-to-waveguide adapter including a discended probe and a tuning post," *IEEE Transactions on Microwave Theory and Techniques*, Vol. 43, 344–349, Feb. 1995.
13. Bui, V. P., X.-C. Wei, and E. P. Li, "An efficient simulation technology for characterizing the ultra-wide band signal propagation in a wireless body area network," *Journal of Electromagnetic Waves and Applications*, Vol. 24, No. 17–18, 2575–2588, 2010.
14. Paulsen, K. D., *Calculation of Power Deposition Patterns in Hyperthermia, Clinical Thermology: Thermal Modeling and Thermal Dosimetry*, Vol. 2, Springer-Verlag, 1988.
15. Marcuvitz, N., *The Institution of Engineering and Technology, Waveguide Handbook*.
16. Hussain, A. and Q. A. Naqvi, "Fractional rectangular impedance waveguide," *Progress In Electromagnetics Research*, Vol. 96, 101–116, 2009.
17. Gabriele, P., T. Ferrara, B. Baiotto, E. Garibaldi, P. G. Marini, G. Penduzzo, V. Giovannini, F. Bardati, and C. Guiot, "Radio hyperthermia for re-treatment of superficial tumours," *Int. J. Hyperthermia*, Vol. 25, 189–98, May 2009.
18. Gong, Y. and G. Wang, "Superficial tumor hyperthermia with flat left-handed metamaterial lens," *Progress In Electromagnetics Research*, Vol. 98, 389–405, 2009.
19. Iero, D., T. Isernia, A. F. Morabito, I. Catapano, and L. Crocco, "Optimal constrained field focusing for hyperthermia cancer therapy: A feasibility assessment on realistic phantoms," *Progress In Electromagnetics Research*, Vol. 102, 125–141, 2010.

20. Carr, J. J., *Practical Antenna Handbook*, 4th edition, McGraw-Hill Professional, 2001.
21. Kumaradas, J. C. and M. D. Sherar, "An edge-element based finite element model of microwave heating in hyperthermia: application to a bolus design," *Int. J. Hyperthermia*, Vol. 18, 441–53, Sep.–Oct. 2002.
22. Van Rhoon, G. C., P. J. Rietveld, and J. Van Der Zee, "A 433 MHz Lucite cone waveguide applicator for superficial hyperthermia," *Int. J. Hyperthermia*, Vol. 14, 13–27, Jan.–Feb. 1998.
23. Frickey, D. A., "Conversions between S , Z , Y , H , $ABCD$, and T parameters which are valid for complex source and load impedances," *IEEE Transactions on Microwave Theory and Techniques*, Vol. 42, 205–211, 1994.
24. Liang, C.-H., Y. Shi, and T. Su, " S parameter theory of lossless block network," *Progress In Electromagnetics Research*, Vol. 104, 253–266, 2010.
25. Pennes, H. H., "Analysis of skin, muscle and brachial arterial blood temperatures in the resting normal human forearm," *Am. J. Med. Sci.*, Vol. 215, 354, Mar. 1948.
26. Mohsin, S. A., N. M. Sheikh, and W. Abbas, "MRI induced heating of artificial bone implants," *Journal of Electromagnetic Waves and Applications*, Vol. 23, No. 5–6, 799–808, 2009.
27. Ebrahimi-Ganjeh, M. A. and A. R. Attari, "Study of water bolus effect on SAR penetration depth and effective field size for local hyperthermia," *Progress In Electromagnetics Research B*, Vol. 4, 273–283, 2008.
28. Gabriel, C., "Compilation of the dielectric properties of body tissues at RF and microwave frequencies," Report N.AL/OE-TR-1996-0037, Occupational and environmental health directorate, Radiofrequency Radiation Division, Brooks Air Force Base, Texas (USA), June 1996.